

Statoliths of the whelk *Buccinum undatum*: a novel age determination tool

Hollyman, Philip; Leng, Melanie; Chenery, Simon; Laptikhovsky, Vladimir;
Richardson, Christopher

Marine Ecology Progress Series

DOI:

[10.3354/meps12119](https://doi.org/10.3354/meps12119)

Published: 28/06/2018

Peer reviewed version

[Cyswllt i'r cyhoeddiad / Link to publication](#)

Dyfyniad o'r fersiwn a gyhoeddwyd / Citation for published version (APA):

Hollyman, P., Leng, M., Chenery, S., Laptikhovsky, V., & Richardson, C. (2018). Statoliths of the whelk *Buccinum undatum*: a novel age determination tool. *Marine Ecology Progress Series*.
<https://doi.org/10.3354/meps12119>

Hawliau Cyffredinol / General rights

Copyright and moral rights for the publications made accessible in the public portal are retained by the authors and/or other copyright owners and it is a condition of accessing publications that users recognise and abide by the legal requirements associated with these rights.

- Users may download and print one copy of any publication from the public portal for the purpose of private study or research.
- You may not further distribute the material or use it for any profit-making activity or commercial gain
- You may freely distribute the URL identifying the publication in the public portal ?

Take down policy

If you believe that this document breaches copyright please contact us providing details, and we will remove access to the work immediately and investigate your claim.

Statoliths of the whelk *Buccinum undatum*: a novel age determination tool

P. R. Hollyman^I, M. J. Leng^{II}, S. R. N. Chenery^{III}, V. V. Laptikhovsky^{IV} and C. A. Richardson^I.

^ISchool of Ocean Sciences, College of Natural Sciences, Bangor University, Menai Bridge, Anglesey, LL59 5AB, UK.

^{II}NERC Isotope Geosciences Facilities, British Geological Survey, Nottingham, NG12 5GG, UK.

^{III}Centre for Environmental Geochemistry, British Geological Survey, Nottingham, NG12 5GG, UK.

^{IV}Centre for Environment, Fisheries and Aquaculture Science (CEFAS), Pakefield Road, Lowestoft, Suffolk, NR33 0HT, UK.

Abstract

The sustainability within the fisheries of the commercially important European whelk, *Buccinum undatum*, has become a major concern through over-exploitation and increased landings in many European coastal shelf seas due to the expansion of export markets to East Asian countries. Current management of *B. undatum* populations is difficult to achieve as several life history traits make them problematic to accurately monitor. The current method of age determination for stock assessment has a low success rate and focuses on the use of putative annual rings on the surface of the organic operculum. Here we validate an annual periodicity of growth ring formation in *B. undatum* statoliths that provides an alternative, reliable and accurate method for determining a whelk's age. Laboratory reared juvenile *B. undatum* of known provenance and age deposited a hatching ring at the time of emergence from their egg capsule and a clearly defined growth ring during February of their first and second years. Stable oxygen isotope profiles around the shells of two adult whelks confirmed annual growth ring deposition by demonstrating seasonal cycles of $\delta^{18}\text{O}$ in the shell that matched the relative position and number of visible growth rings in the statolith. Validation of annually-resolved statolith growth rings will for the first time, provide fisheries scientists with a tool to determine the age structure of *B. undatum* populations and allow analytical stock assessments that will enable informed decisions for future management practices of whelk fisheries.

Keywords: *Buccinum undatum*, statoliths, age determination, fisheries monitoring, oxygen isotope, Raman Spectroscopy, Sclerochronology

Introduction

The common whelk *Buccinum undatum*, is a commercially important species of marine gastropod fished in the coastal waters of the U.K. and across Northern Europe. In 2015 the UK landings of *B. undatum* by UK vessels totalled 20,900 tonnes with a value at first sale of £18.7 million (MMO, 2016). A large proportion of the whelk landings in the UK and Ireland supply an export market to East Asia that has grown steadily since the mid-1990s (Fahy *et al.*, 2000) in response to recent increases in consumer demand which has driven the expansion of the fishery. However, declines in the number of whelks caught have been noted across European waters (Jersey - Shrives *et al.*, 2015; Ireland - Fahy *et al.*, 2005; North Sea/Netherlands - Ten Hallers-Tjabbes *et al.*, 1996) and have caused several local Inshore Fishery and Conservation Authorities (IFCA's) recently to implement restrictions such as pot and/or catch limits and the number of permits issued (Devon & Severn IFCA, 2016, Eastern IFCA, 2016 and Kent & Essex IFCA, 2016).

The reliable assessment of age and longevity of *B. undatum* is problematic for fisheries scientists, due to *B. undatum* having several life history traits which make them difficult to monitor at a population level. The lack of a planktonic larval stage and a relatively inactive adult lifestyle with no apparent migration (Pálsson *et al.*, 2014) has led to the formation of discrete stocks which are then vulnerable to overexploitation (Fahy *et al.*, 2000). In many studies these stocklets have been observed to show clear genetic and morphometric differences (e.g. Weetman *et al.*, 2006; Shelmerdine *et al.*, 2007; Magnúsdóttir, 2010), including size at maturity which can also differ markedly between sites (McIntyre *et al.*, 2014; Haig *et al.*, 2015; Shrives *et al.*, 2015).

To resolve this conundrum a reliable ageing method needs to be established for *B. undatum* so that accurate population age assessments and analytical stock assessments can be undertaken. The currently accepted method used by fisheries scientists, and validated by Santarelli and Gros (1985), determines the age of whelks by reading growth rings on the operculum, an organic 'shield' that is used to protect the shell aperture when the animal withdraws into its shell. This was achieved by

matching cycles in oxygen isotope composition from the shell to the numbers of growth rings observed on the opercula. However, this method traditionally has had a low success rate owing to the poor clarity of the rings, a problem highlighted by Kideys (1996), who reported that only 16%, from a total of 10,975 opercula examined in whelks from the Isle of Man, U.K., having “clear and readable” rings, with a further 32% having “readable” rings, leading to 48% of the samples being discarded. More recently, similar low levels of readability were found in several sites around the UK (Lawler, 2013). The exclusion of large portions of samples due to poor clarity of the rings is likely to have biased the data; the constructed population growth curves were highly variable, presumably due to the ambiguity of the operculum readings.

Since whelks are becoming increasingly exploited there is an urgent scientific need to underpin the fisheries stock assessment of their populations with accurate data concerning the age of individuals and their growth rates. For many mollusc species, the age of an individual can be determined by counting the annual growth lines present in longitudinal shell sections (See Richardson, 2001, for review). This is particularly applicable to bivalve molluscs, but in gastropods this is not possible because there are often no obvious annual growth rings on or contained within their shells. Gastropod shells are also often problematic to analyse via sectioning as their coiled morphology makes it difficult to obtain a single clear growth axis using this technique.

Mollusc shells are repositories of information about the past environmental history of shell growth and contain within the carbonate of their shells biogenic trace elements and oxygen isotopes at ratios ($^{18}\text{O}/^{16}\text{O}$, described as $\delta^{18}\text{O}$) which are incorporated into the shell matrix at equilibrium during mineralisation (Wilbur & Saleuddin 1983; Wheeler 1992). Seawater temperature at the time of shell formation can be reconstructed from the gastropod shell throughout ontogeny by determining $\delta^{18}\text{O}$ along the growing axis of the shell e.g. *Rapana venosa* (Kosyan & Antipushina, 2011) and *Conus ermineus* (Gentry *et al.*, 2008). The empirical fractionation of oxygen isotopes in mollusc carbonates with changes in temperature are well known (e.g. Epstein *et al.*, 1953). Oxygen isotopes are sourced

from H₂O and CO₂ during shell formation (Leng and Lewis, 2016); a more negative value of $\delta^{18}\text{O}$ reflects warmer seawater temperatures whilst a more positive value is indicative of cooler seawater temperatures (Grossman & Ku, 1986) at a constant $\delta^{18}\text{O}$ of seawater. Sampling the shell carbonate at known intervals along the whorled axis of the shell and determining seasonal changes in $\delta^{18}\text{O}$ allows the age (seasonality) of the shell to be determined. This approach is not suitable for large scale ageing of whelk due to the cost of analysing the potentially huge numbers of samples needed to accurately reconstruct the seasonality across a significant number of shells.

In lieu of being able to directly use the shells or opercula to estimate age, an alternative age registering structure was sought; whelks contain an accretory hard structure called a statolith which is the focus of this paper. Statoparticles (such as statoliths) are structures that are integral to the nervous system of a diverse range of animal groups including the Polychaeta (Beesley *et al.*, 2000), Holothuroidea (Ehlers, 1997), Crustacea (Espeel, 1985) and several classes of the Mollusca e.g. the Bivalvia (Morton, 1985), Gastropoda (Barroso *et al.*, 2005; Chatzinikolaou & Richardson 2007; Galante-Oliveira *et al.*, 2013) and Cephalopoda (Arkhipkin, 2005). They are used in gravity perception and are contained within a statocyst, which detects movement of the statoparticle, indicating a change in orientation (Chase, 2002). Commonly composed of calcium carbonate they have a wide ranging morphology across the phylum in which they are found. The statoparticles of gastropods are often singular, roughly spherical granules called statoliths (Richardson, 2001; Galante-Oliveira *et al.*, 2013). Gastropod statoliths can contain rings that are deposited annually e.g. *Nassarius reticulatus* (Barroso *et al.*, 2005), *Neptunea antiqua* (Richardson *et al.*, 2005b) and *Polinices pulchellus* (Richardson *et al.*, 2005a) and are an archive of biota life history, containing information about the age and the seasonal temperature cycles (Richardson *et al.*, 2005a, Galante-Oliveira *et al.*, 2015) and their transition from a planktonic pelagic larval lifestyle to a benthic existence (Barroso *et al.*, 2005; Richardson *et al.*, 2005a; Chatzinikolaou & Richardson 2007). Once the rings in the statolith have been deciphered, information about a gastropod's life history can be extracted to understand their ontogenic growth. Thus they are potentially an invaluable resource for

fisheries scientists who could use this information to assess population age structure of commercially important gastropod species such as *B undatum*.

Here we demonstrate for the first time that growth rings in the statoliths of *B undatum* are annually deposited like those within the opercula and can be used for the reliable age estimation of the species. The timing of statolith growth ring formation was determined in whelks of known age and life history that had been reared in the laboratory under ambient seawater temperatures for two years following their emergence from egg capsules. The structure of the statoliths was also investigated to determine their general morphology and mineralogical composition. We then used shell $\delta^{18}\text{O}$ profiles drilled from around the whorl and compared these data with the matching whelk statoliths growth lines.

Materials and methods

Field collection: Approximately 200 whelks (>25mm shell length) were trapped and collected in February 2015 from a site in the Menai Strait (North Wales, U.K., 53.235556, -4.141835 – decimal degrees, depth 10-11.5m) using a string of 3 baited scientific inkwell pots laid for 24 hours. The drainage holes in the pots were covered with 3mm mesh and the whelk catch was not riddled (the process used by fishermen to remove undersized whelks) to ensure all size classes were retained for analysis. Dispensation for the landing of undersized whelks (<45mm) was granted by the Welsh Government (disp#004). Once collected, whelks were frozen until required, whereupon they were thawed and the body removed from their shells using forceps by gently pulling on the foot to detach the collumellar muscle. Shell height (aperture to spire length) was measured to the nearest 1mm using Vernier callipers, total body weight was recorded to the nearest 0.1g and reproductive maturity assessed using the scale of Haig *et al.* (2015). The body of each whelk were re-frozen for later statolith extraction.

Laboratory experiment: This experiment was designed to study the formation of the whelk statolith during ontogeny and to determine the timing of growth ring formation. Seven whelk egg masses that had been laid naturally in an intertidal location at Tal-y-Foel (53.158512, -4.279493 – decimal degrees), in the Menai Strait were collected in November 2013 and 2014. Egg masses were transported to the laboratory and held in aquaria supplied with flowing ambient seawater from the Menai Strait. Approximately 2 months later juvenile whelks hatched directly from the egg capsules and were reared for 1 year (2014 hatching) and 2 years (2013 hatching) under an approximate 10:14hr light/dark cycle and fed regularly thrice weekly with small pieces of frozen and thawed mackerel *Scomber scombrus*. Each month for 24 months, ten whelks were removed and frozen for later statolith extraction.

Stolith extraction and ageing: Selected individuals of both frozen field caught adult and laboratory reared juvenile whelks were thawed (3hrs) and the body bisected (Figure 1a). Each half of the whelk body was examined under a low power binocular microscope to locate, dissect and then remove, using fine forceps (0.10 x 0.06mm tip), a pair of statocyst sacs (left and right side) each containing a statolith (Figure 1b). Incident illumination as well as transmitted light were used during the dissections and highlighted the statoliths as small shadows beneath the cerebral ganglion (Fig. 1c). The <0.75mm statocysts were transferred to a watch glass with a drop of Milli-Q® ultrapure water (Merck Millipore), torn open and the statoliths removed using a hypodermic needle (0.5 mm diameter). Where necessary, each statolith was cleaned of any adhering tissue by immersion in 20% sodium hydroxide (NaOH) for 30 minutes and rinsed in Milli-Q® quality water. Once the statoliths had air-dried they were mounted on a microscope slide using Crystalbond™ 509 thermoplastic resin and imaged under a Meiji Techno MT8100 microscope with a Lumenera Infinity 3 microscope camera at 40x magnification. This allowed the visualisation of the statolith growth rings that could then be counted and statolith diameter measured using ImageJ (version 1.48, Ferreira & Rasband 2012; Fig. 2).

Scanning Electron Microscopy (SEM): Several statoliths from the right and left side of small and large whelks were selected for structural analysis. Each statolith was mounted in Crystalbond™ 509 on an aluminium SEM stub and imaged as above. The statolith was ground by hand to the central plane using progressively finer 400, 1200, 2500 & 4000 silicon carbide grinding papers lubricated with Milli-Q® quality water. Each statolith was finally polished with a 1 µm diamond suspension gel and thoroughly cleaned with detergent and water and dried before submersion in 0.1M hydrochloric acid for 2 minutes to etch the exposed statolith surface. The exposed and etched statolith surfaces were then imaged using a FEI QUANTA 600 environmental scanning electron microscope (SEM) operated in low vacuum mode, with an electron beam accelerating voltage of 12.5 - 15 kV, a beam probe current of 0.14 - 0.26 nA, and a working distance of 10.6-10.9 mm.

Micro-Raman Spectroscopy (MRS): Raman spectroscopy allows differentiation between the polymorphs of CaCO₃ (amorphous CaCO₃, calcite, aragonite and vaterite) by focusing a laser light onto the statolith surface. Inelastic scattering of the incident light occurs after interacting with the sample structure due to interaction with the vibrational levels of the composite molecules causing a shift in the wavelength of the measured scattered photons (Raman shift) (Higson, 2006). The wavelength shifts of the spectra are predictable in position and intensity for different substances. For CaCO₃, two main wavelength regions of the spectra are of interest, peaks in the 100–350 cm⁻¹ range pertain to interaction with features of the external lattice structure whereas peaks in the 600–1800 cm⁻¹ relate to interactions with the internal molecular planes (Parker *et al.*, 2010). To determine the statolith composition, individual statoliths were fractured using fine tipped forceps (0.10 x 0.06mm tip) to reveal the inner growth axis and analysed with MRS (Reinshaw InVia Raman-Microscope) at the Diamond Light Source, Harwell, UK. The MRS consisted of a 473 nm laser at a power of 15 mW and focussed using a lens with a magnification of 20x; a grating with 2400 lines/mm⁻¹ and a pinhole size of 100 µm were used for spectra acquisition. The spectra were acquired between 100 and 3200 cm⁻¹. Three sample spots were taken approximately equidistant along the interior growth axis of three statoliths from the central nucleus to the outer edge although

only the results from one statolith are presented. Synthetic calcite and speleothem aragonite standards (Brinza *et al.*, 2014) were analysed prior to and after statolith analyses and the resulting Raman spectra adjusted using a polynomial background correction. Following MRS, the fractured statolith surface was imaged using SEM to obtain a detailed image of the sampled surface.

Isotope Ratio Mass Spectrometry (IRMS): The outer periostracum and any adhering material were cleaned from the shells of an adult male and female whelk collected from the Menai Strait using a stiff bristled brush and tap water and air-dried. The shell surface was abraded using a 1mm diamond burr attached to a Dremel® 4000 to remove any contamination from the shell surface. A sampling axis around the entire whorled growth was marked out close to the shoulder of the shell whorl with 1mm notations along its length. 1x10mm tracks were drilled at a resolution of 2 mm at the apex and most recently formed whorl, the oldest and youngest parts of the shell, then at 4mm for the central portion where growth is fastest, in line with the visible growth striations. Care was taken to only sample the outer nacreous layer of the shell and not drill into the inner nacreous layers which are deposited at a later time. The drilled CaCO₃ samples were collected on small square (2x2 cm) sheets of greaseproof paper transferred to a labelled 0.5ml Eppendorf tube. This sampling strategy was extended as close to the tip of the shell as possible, however, in all cases the earliest shell growth (top 1-1.5cm) could not be sampled owing to shell damage and resolution of drilling.

Approximately 50 – 100 µg of powdered carbonate sample were used for isotope analysis using an IsoPrime dual inlet mass spectrometer plus Multiprep device (at the British Geological Survey, Keyworth, UK). Weighed samples were added to glass vials which were then evacuated and anhydrous phosphoric acid (H₃PO₄) was added to each sample at 90°C. The samples were left to digest for 15 minutes and the expressed gas collected, cryogenically cleaned to remove any moisture and passed into the mass spectrometer. Isotope values ($\delta^{13}\text{C}$, $\delta^{18}\text{O}$) are reported as per mille (‰) deviations of the isotopic ratios ($^{13}\text{C}/^{12}\text{C}$, $^{18}\text{O}/^{16}\text{O}$) calculated to the VPDB scale using a within-run laboratory standard (KCM) calibrated against NBS-19. The aragonite-acid fractionation factor applied

to the gas values was 1.00855 (Sharma & Clayton, 1965). A drift correction is applied across the run, calculated using the standards that bracket the samples. The Craig correction was also applied to account for the influence of $\delta^{17}\text{O}$ within the sample (Craig, 1967). The average analytical reproducibility of the standard calcite (KCM) is 0.05‰ for $\delta^{13}\text{C}$ and $\delta^{18}\text{O}$. The resulting ($^{18}\text{O}/^{16}\text{O}$ ratio) data were treated with a 5-point Savitsky-Golay smoothing filter (Steiner *et al.*, 1972). The $\delta^{13}\text{C}$ data is not presented here.

Results

Statolith location and morphology: Each whelk contains two statocysts in the tissues of its foot, each containing a single roughly spherical statolith (st) (<0.75mm in diameter) (Fig. 1b). Orientation of the statolith in resin in a dorsal/ventral position shows a circular outline shape and is the optimum position to view and measure the visible growth rings (Fig. 2a). Laterally the statolith has an oval shape (Fig. 2b) and has a dorso-ventrally compressed spherical shape where the rings are less clear. Thus to maintain consistency and to maximise the visibility of the rings all analyses/images were undertaken from statoliths orientated in a dorsal-ventral view.

The relationship between Statolith Diameter (StD) and Shell Length (SL) was shown to display a power relationship (Fig. 3a). This was investigated further using the ‘smatr’ package in R to analyse the log10 transformations of each variable (Fig. 3a inset). A significant correlation was found between the two variables ($p < 0.001$) and with a slope of 0.438 (0.432 and 0.443 lower and upper 95% confidence intervals respectively). This shows the relationship has negative allometry, indicating that statoliths and shells do not grow proportionally. Instead the growth of the statoliths decreases in comparison to the shell length over time. This results in smaller whelks having proportionally larger statoliths in comparison to shell length. The data in Fig. 3a closely fit the line for whelks <60mm allowing estimates of shell length to be determined from the diameter of the rings. However, above this size there is wide variation in statolith diameter. By measuring the statolith diameter at successive rings for whelks <60mm it is feasible to reconstruct shell length at each ring.

Figure 3b, shows the relationship between StD and age (ascertained from statolith rings in field caught whelks) has been fitted with a von Bertalanffy growth curve ($R^2 = 0.90$). Although there is a strong relationship, there are large amounts of overlap between ages. The clarity of the statoliths was also very high with the vast majority of samples included in the analysis ($n=800$). 48.6% of the samples were classed as “clear and readable” and a further 43% as “readable (using the same criteria as Kideys, 1996), thus only 8.4% of samples were excluded.

Statolith Structure: The broken statolith shown in Figure 4a is composed of aragonite. All three of the analysed statoliths displayed the characteristic peaks for aragonite. The Raman spectra extracted between 100 and 750 cm^{-1} demonstrate a coincidence of peaks at 151 cm^{-1} , 183 cm^{-1} , 206 cm^{-1} and a wide peak at 702-706 cm^{-1} for both sample spots 1-3 from the statolith and the aragonite standard (Figure 4b). A shoulder is also visible on the 151 cm^{-1} peak at 143 cm^{-1} . By contrast the calcite standard peaks at 155 cm^{-1} , 281 cm^{-1} and 712 cm^{-1} indicate that this statolith contains no trace of calcite. Figure 4c shows an additional peak between 2850 and 3000 cm^{-1} for the three sample spots. Peaks in this range are thought to be indicative of C-H functional groups found within organic matter (Smith & Dent, 2005) thus likely indicative of the presence of an organic component within the crystal matrix. Figure 5 shows the agreement between the visible rings in the optical microscope (OM) image of a whole statolith (Fig. 5a) and the exposed acid etched SEM image of the central plane of the paired statolith (Fig. 5b). The clarity of the rings in Figure 5b suggests that a clear structural change has occurred during the formation of a growth ring.

Hatching ring and growth ring formation: The inner opaque area seen in Figure 5a signifies the period of development in the egg culminating in the formation of a hatching ring (HR). The hatching ring can also be seen and appears in January when these animals hatched (Figure 6a, b, c & d). For the 2013 juvenile cohort the hatching ring was deposited at a statolith diameter of $53.6 \pm 4\mu\text{m}$ ($\pm 1\text{SD}$, $n=30$) and for the 2014 cohort at $55.1 \pm 6\mu\text{m}$ ($\pm 1\text{SD}$ $n=30$). The data from the two cohorts were not significantly different (independent t-test, $p = 0.1$). The central opaque area (larval growth) seen

in Figure 5a is followed by a less opaque region containing weak and diffuse rings. This pattern is also mirrored in Figure 6 which shows the ontogenetic development of statoliths removed from laboratory reared animals of different ages between 2 weeks and 2 years. Clear disturbance rings can be seen in the increment following hatching ring deposition and are a common feature of adult statoliths. The clear year 1 ring in the statolith in Figure 6d marks a colour change from brown to light brown and was deposited in February during the coldest part of the annual temperature cycle. A similar positioned ring can be seen in Figure 5a, signifying the first annual ring formation. The colour change is regularly seen in statoliths taken from “field caught” adult whelks and is a good indicator of the position of the first annual growth ring. Following deposition of the slightly unclear first annual ring, subsequent annual rings are clearly delineated in both the optical microscope and SEM images of Figure 5a & b. Disturbance rings, that are a common feature of the statoliths in younger whelks, are typically much weaker in definition than the clear annually-resolved rings.

Annual growth ring validation: Figure 7 shows the coincidence between the statoliths ring position (7c & f) and maximum values in the shell $\delta^{18}\text{O}$ cycles (7a & d). Maximum $\delta^{18}\text{O}$ represents minimum seawater temperatures. The three $\delta^{18}\text{O}$ minima in the female shell (a) match the position of the three statolith rings (c) and the four maxima seen in the male shell (d) match the four statolith rings (f). In both shells the tip of the apex was not sampled, represented by the grey hatch area in Figure 7a & d, and the point at which sampling ceased is indicated by a black arrow (Fig. 7b and e).

Discussion

This study validates for the first time the annual periodicity of growth rings found within the statoliths of the common whelk, *Buccinum undatum*; as well as investigating their structure and composition. This was achieved using a combination of laboratory rearing of juvenile specimens and geochemical analysis of both statoliths and shells from wild collected adults. The validation of the annual growth lines as a reliable ageing tool will provide an alternative to the currently used and often unreliable operculum.

Visualization, interpretation and timing of statolith ring formation: In a previous study following extraction and statolith cleaning, Richardson *et al.* (2005a) hand-ground and polished the statoliths of the neogastropod *Neptunea antiqua* to observe the growth rings. However in the current study when *B. undatum* statoliths were hand-ground (using the above described methods for SEM preparation) and observed in the optical transmitted light microscope, weaker disturbance rings became more apparent and often obscured the earliest annual growth rings due to the removal of the overlying statolith structure which often masked them. However, when a whole statolith was observed weaker lines were less apparent and this approach was adopted throughout the study.

A single, clear growth ring was deposited annually within the statoliths of the laboratory reared juveniles during February and March when seawater temperatures were minimal in the Menai Strait. Female *B. undatum* lay egg capsules in which larvae develop and juveniles hatch directly leaving their egg capsules without a planktonic larval stage. The first identifiable diffuse statolith ring deposited can be termed a “hatching ring”, formed as the juveniles emerge from their capsules. The hatching ring has a similar position in the statolith to the settlement ring in statoliths from *Polinices pulchellus* (Richardson *et al.*, 2005b) and *Nassarius reticulatus* (Barroso *et al.*, 2005; Chatzinikolaou & Richardson 2007)) that hatch from egg capsules and undergo a planktonic larval existence prior to settlement. Thus importantly, these two kinds of juvenile rings in gastropods with different early life strategies represent the same life history event i.e. the transition from larvae to juvenile. Whilst hatching ring diameters in reared *B. undatum* juveniles are fairly constant (53.6 to 55.1µm), it has been shown that maternal size directly influences egg capsule size and subsequently juvenile hatching size, which in turn can also be mediated by intra-capsular cannibalism (Nasution, 2003; Nasution *et al.*, 2010, Smith & Thatje, 2013). Therefore, in a population with larger than average sized whelks, the hatching ring will be larger than the average observed here. A strong relationship exists between statolith diameter and shell length, however with wide variation in statolith diameters in large (>60mm) and older whelks means that it is not possible to estimate an older whelk’s age solely from statolith size. The age of each whelk must be determined by counting

the number of annually-resolved statolith rings. The annual periodicity of the growth rings was further validated with the reconstruction of $\delta^{18}\text{O}$ profiles from shells (Fig. 7). This is the same method used by Santarelli & Gros (1985) to validate the observable growth rings in the opercula. However, in this study a higher sampling resolution was used, producing more clearly defined $\delta^{18}\text{O}$ cycles that are directly overlaid on the visible growth rings of the statolith. Santarelli and Gros (1985) did not demonstrate the ages of the animals from the opercula.

Stanolith composition: The statoliths of *B. undatum* are aragonite as shown by Raman spectra with no visible trace of calcite. There was close agreement between the aragonite standard and the sample spots taken from the statolith, several of the reported Raman spectra peaks differed by 1-3 cm^{-1} compared with those reported in the literature (see Parker *et al.*, 2010). It is probable that the difference between the observed statolith spectra peaks and the published spectra is the presence of trace elements such as Mg^{2+} substituting for Ca^{2+} within the lattice and distorting it (Parker *et al.*, 2010). This would explain why the synthetic calcite standard exhibited all of the expected peaks whereas the sample spots and the speleothem aragonite standard (which can contain trace elements, Finch *et al.* 2001) did not. The Raman spectra of the sample spots also exhibited a diffuse band between 2850 and 3000 cm^{-1} which likely indicates the presence of structural organic matter within the CaCO_3 matrix. All three of the spot samples showed a peak in the spectra likely indicating the presence of organic matter throughout the statolith matrix, although the most intense peak was observed when the structure of a growth ring was coincidentally analysed (spot 3 on the statolith). A similar conclusion was reached by Galante-Oliveira *et al.*, (2014) who observed similar spectra in the statoliths of *Nassarius reticulatus*. If the Raman peaks represent differences in the concentration of organic matter present in different parts of the statolith then this will aid in interpreting the distribution of elements such as Sr and Mg in the statolith. In *N. reticulatus* annual cycles of Sr-Ca ratios were found to correspond with the visible growth rings (Galante-Oliveira *et al.*, 2015) with minimum ratios associated with the rings and maximum concentrations present in the increments between adjacent rings. Schone *et al.* (2010) has demonstrated the role of organic material in

bivalve shells in regulating the control of biogenic element incorporation into the shell structure, highlighting that insoluble organic matter present aragonitic shell of *Arctica islandica* is significantly enriched in Mg and depleted in Sr.

Implications for fisheries: With the development of this ageing technique for such a commercially important species, the construction and comparison of population growth curves can be easily implemented on a potentially large scale. Vast improvements over the operculum age determination method have been shown, with a decrease in discarded samples from 48% down to 8.4% and an increase in useable samples from 52% to 91.6%. Whilst the methodology for statolith extraction and analysis is potentially more time consuming than the use of opercula, the huge increase in reliability and decrease in potential sample bias (from large discards) is clear.

Summary

Here, an annually-resolved periodicity of growth ring formation in whole resin-mounted statoliths from *Buccinum undatum* was validated by comparison with seasonally-collected and laboratory-reared juvenile whelks of known age and from similarities between growth rings and the $\delta^{18}\text{O}$ cycles in their shells. This validated novel age determination tool (using the statoliths) can be used to accurately reconstruct the population structure and population growth rates of *B. undatum* and the technique will now be available for fisheries scientists to undertake stock assessments of whelk populations European-wide to determine both size at age, and age at reproduction. These are both metrics that will aid in future management decisions. The statoliths present a viable alternative to the “difficult to use” opercula. *Buccinum undatum* statoliths are composed of aragonitic calcium carbonate and their structure determined by Raman-Microscopy has revealed variations in organic matter throughout the statolith that might have implications for the way in which biogenic elements are incorporated into the organic lattice of the statolith. Overall we conclude understanding differences in the age, growth rate and distributions of whelks in coastal waters will add

immeasurably to understanding how to manage and conserve these important scavengers in coastal zones.

Acknowledgements

This work was supported through a Bangor University/CEFAS partnership PhD scholarship to PH. We are grateful to Gwynne Parry-Jones for collecting the *Buccinum undatum* from the Menai Strait. The IRMS analyses were supported by a NERC Isotope Geosciences Facilities Steering Committee (IP-1527-0515) award and thanks to Hilary Sloane for technical support. Access to the Reinshaw Raman-Microscope was made possible through a rapid access request to the Diamond Light Source (SP13616-1). Production of the SEM micrographs would not have been possible without the help of Dr Lorraine Field (BGS) and Dr. Andy Marriott (BGS). A number of colleagues and students, Richard Patton, Charlotte Colvin, Helène Bonici, Anton Antonov and Devaney Werrin are acknowledged for their invaluable help with animal husbandry. We also thank Dr. Ewan Hunter and Dr. Andy Marriott, and three anonymous reviewers whose comments improved the manuscript greatly.

M. Leng and S. Chenery publish with the permission of the Director British Geological Survey and PH is registered as a BUFI student within BGS.

References

- Arkhipkin AI (2005) Statoliths as 'black boxes' (life recorders) in squid. *Mar Freshwater Res* 56:573-583
- Barroso CM, Nunes, M, Richardson CA, Moreira MH (2005) The gastropod statolith: a tool for determining the age of *Nassarius reticulatus*. *Mar Biol* 146:1139–1144
- Beesley PL, Ross GJB, Glasby CJ (eds) Polychaetes & Allies: The Southern Synthesis. Fauna of Australia. Vol. 4A Polychaeta, Myzostomida, Pognophora, Echiura, Sipuncula. CSIRO publishing, Melbourne.
- Brinza L, Schofield PF, Mosselmans JFW, Donner E, Lombi E, Paterson D, Hodson ME (2014). Can earthworm-secreted calcium carbonate immobilise Zn in contaminated soils? *Soil Biol Biochem* 74:1-10.
- Chase R (2002) Behaviour & its neural control in gastropod molluscs. Oxford University Press, New York

384 Chatzinikolaou E, Richardson CA (2007) Evaluating the growth and age of the netted whelk *Nassarius*
385 *reticulatus* (gastropoda: nassaridae) from statolith growth rings. Mar Ecol Prog Ser
386 342:163-176

387 Craig H (1957) Isotopic standards for carbon and oxygen & correction factors for mass spectrometric
388 analysis. Geochim Cosmochim Acta 12:133-149

389 Devon & Severn IFCA (2016) <http://www.devonandsevernifca.gov.uk/> (accessed 1/7/16)

390 Eastern IFCA (2016) <http://www.eastern-ifca.gov.uk/> (accessed 1/7/16)

391 Ehlers U (1997) Ultrastructure of the Statocysts in the Apodous Sea Cucumber *Leptosynapta*
392 *inhaerens* (Holothuroidea, Echinodermata). Acta Zool – Stockholm 78 (1):61-68

393 Epstein S, Buchsbaum JR, Lowenstam HA, Ukey HC (1953) Revised carbonate-water isotopic
394 temperature scale. Bull Geol Soc Am 64:1315-1326

395 Espeel M (1985) Fine structure of the statocyst sensilla of the mysid shrimp *Neomysis integer* (Leach,
396 1814) (Crustacea, Mysidacea). J Morphol 186:149-165

397 Fahy E, Carroll J, O'Toole M, Barry C, Hother-Parkes L (2005) Fishery associated changes in the whelk
398 *Buccinum undatum* stock in the southwest Irish Sea, 1995-2003. Irish Fisheries
399 Investigations 15, Marine Institute, Dublin.

400 Fahy E, Masterson E, Swords D, Forrest N (2000) A second assessment of the whelk fishery *Buccinum*
401 *undatum* in the southwest Irish Sea with particular reference to its history of management
402 by size limit. Irish Fisheries Investigations 6, Marine Institute, Dublin.

403 Ferreira T, Rasband W (2012) ImageJ User Guide.

404 Finch AA, Shaw PA, Weedon GP, Holmgren K (2001) Trace element variation in speleothem
405 aragonite: potential for palaeoenvironmental reconstruction. Earth and Planet Sci Lett
406 186:255-267

407 Fretter V, Graham A (1994) British Prosobranch Molluscs. The Ray Society, London.

408 Galante-Oliveira S, Marçal R, Espadilha F, Sá M, Abell R, Machado J, Barroso C (2015) Detection of
409 periodic Sr Ca⁻¹ cycles along gastropod statoliths allows the accurate estimation of age.
410 Mar Biol 162:1473-1483. doi 10.1007/s00227-015-2684-y

411 Galante-Oliveira S, Marçal R, Guimarães F, Soares J, Lopes JC, Machado J, Barroso C (2014)
412 Crystallinity and microchemistry of *Nassarius reticulatus* (Caenogastropoda) statoliths:
413 towards their structure stability and homogeneity. J Struct Biol 186:292–301.
414 doi:10.1016/j.jsb.2014.03.023

415 Galante-Oliveira S, Marçal R, Ribas F, Machado J, Barroso C (2013) Studies on the morphology and
416 growth of statoliths in Caenogastropoda. J Mollus Stud 79:340–345.
417 doi:10.1093/mollus/eyt028

418 Gentry DK, Sosdian S, Grossman EL, Rosenthal Y, Hicks D, Lear CH (2008) Stable isotope and Sr/Ca
419 profiles from the marine gastropod *Conus ermineus*: testing a multiproxy approach for

420 inferring paleotemperature and Paleosalinity. *Palaios* 23:195-209 doi:
 421 10.2110/palo.2006.p06-112r

422 Grossman EL, Ku T (1986) Oxygen and carbon isotope fractionation in biogenic aragonite:
 423 Temperature effects. *Chem Geol* 59:59-74. doi: 10.1016/0168-9622(86)90057-6

424 Haig JA, Pantin, JR, Murray LG, Kaiser MJ (2015) Temporal and spatial variation in size at maturity of
 425 the common whelk (*Buccinum undatum*). *ICES J Mar Sci* 72(9):2707-2719.
 426 doi:10.1093/icesjms/fsv128

427 Higson SPJ (2006) *Analytical Chemistry*. Oxford University Press, New York.

428 Kent & Essex IFCA (2016) <http://www.kentandessex-ifca.gov.uk/> (accessed 1/7/16)

429 Kideys AE (1996) Determination of age and growth of *Buccinum undatum* L. (Gastropoda) off
 430 Douglas, Isle of Man. *Helgol. Meeresunters.* 50 (3):353–368.

431 Kosyan AR, Antipushina ZA (2011) Determination of *Rapana venosa* individuals' ages based on the
 432 $\delta^{18}\text{O}$ dynamics of the shell carbonates. *Oceanology* 51:1021-1028.
 433 doi:10.1134/S0001437011060075

434 Lawler A (2013) Determination of the size of maturity of the whelk *Buccinum Undatum* in English
 435 waters – Defra Project MF0231

436 Leng MJ, Lewis JP (2016) Oxygen isotopes in Molluscan shell: Applications in environmental
 437 archaeology. *Environmental Archaeology* 21(3):295-306

438 Magnúsdóttir H (2010) The common whelk (*Buccinum undatum* L.): Life history traits and population
 439 structure. Master thesis. University of Iceland, Reykjavik.

440 Marine Management Organisation (2016) UK Sea Fisheries Statistics 2015. Office for National
 441 Statistics, London. 156 pp.

442 McIntyre R, Lawler A, Masefield R (2015) Size of maturity of the common whelk, *Buccinum undatum*:
 443 Is the minimum landing size in England too low? *Fish Res* 162:53–57.
 444 doi:10.1016/j.fishres.2014.10.003

445 Morton B (1985) Statocyst structure in the Anomalodesmata (Bivalvia). *J Zool* 206:23–34.
 446 doi:10.1111/j.1469-7998.1985.tb05633.x

447 Nasution S (2003) Intra-capsular development in marine gastropod *Buccinum undatum* (Linnaeus
 448 1758). *Jurnal Natur Indonesia* 5:124–128

449 Nasution S, Roberts D, Farnsworth K, Parker GA, Elwood RW (2010) Maternal effects on offspring
 450 size and packaging constraints in the whelk. *J Zool* 281:112-117. doi:10.1111/j.1469-
 451 7998.2009.00681.x

452 Parker JE, Thompson SP, Lennie AR, Potter J, Tang CC (2010) A study of the aragonite–calcite
 453 transformation using Raman spectroscopy, synchrotron powder diffraction and scanning
 454 electron microscopy. *Cryst Eng Comm* 12:1590–1599. doi: 10.1039/b921487a

455 Pálsson S, Magnúsdóttir H, Reynisdóttir S, Jónsson ZO, Örnólfssdóttir EB (2014) Divergence and
 456 molecular variation in common whelk *Buccinum undatum* (Gastropoda: Buccinidae) in

457 Iceland: a trans-Atlantic comparison. Biol J Linn Soc Lond 111:145–159.
 458 doi:10.1111/bij.12191

459 Richardson CA (2001) Molluscs as archives of environmental change. Oceanogr Mar Biol 39:103–164

460 Richardson CA, Kingsley-Smith PR, Seed R, Chatzinikolaou E (2005b) Age and growth of the naticid
 461 gastropod *Polinices pulchellus* (Gastropoda: Naticidae) based on length frequency analysis
 462 and statolith growth rings. Mar Biol 148:319–326. doi:10.1007/s00227-005-0072-8

463 Richardson CA, Saurel C, Barroso CM, Thain J (2005a) Evaluation of the age of the red whelk
 464 *Neptunea antiqua* using statoliths, opercula and element ratios in the shell. J Exp Mar Biol
 465 Ecol 325:55–64. doi:10.1016/j.jembe.2005.04.024

466 Santarelli L, Gros P (1985) Age and growth of the whelk *Buccinum undatum* L. (Gastropoda:
 467 Prosobranchia) using stable isotopes of the shell and operculum striae. Oceanol Acta 8
 468 (2):221–229

469 Schöne BR, Zhang Z, Jacob D, Gillikin DP, Tütken T, Garbe-Schönberg D, McConnaughey T, Soldati A
 470 (2010) Effect of organic matrices on the determination of the trace element chemistry (Mg,
 471 Sr, Mg/Ca, Sr/Ca) of aragonitic bivalve shells (*Arctica islandica*) – Comparison of ICP-OES
 472 and LA-ICP-MS data. Geochem J 44:23–37

473 Sharma T, Clayton RN (1965) Quoted in: Friedman I and O’Neil JR, 1977. Compilation of stable
 474 isotope fractionation factors of geochemical interest. Fleischer (Ed), Data of Geochemistry,
 475 6th Ed. United States Geological Survey, Professional Paper 440-KK

476 Shelmerdine RL, Adamson J, Laurenson CH, Leslie B (2007) Size variation of the common whelk,
 477 *Buccinum undatum*, over large and small spatial scales: potential implications for micro-
 478 management within the fishery. Fish Res 86:201–206. doi:10.1016/j.fishres.2007.06.005

479 Shrives JP, Pickup SE, Morel GM (2015) Whelk (*Buccinum undatum* L.) stocks around the Island of
 480 Jersey, Channel Islands: Reassessment and implications for sustainable management. Fish
 481 Res, 167: 236–242. doi: 10.1016/j.fishres.2015.03.002

482 Smith E, Dent G (2005) Modern Raman Spectroscopy – A Practical Approach. John Wiley & Sons, Ltd,
 483 England.

484 Smith KE, Thatje S (2013) Nurse egg consumption and intracapsular development in the common
 485 whelk *Buccinum undatum* (Linnaeus, 1758). Helgo Mar Res 67:109–120.

486 Steiner J, Termonia Y, Deltour J (1972) Comments on Smoothing and Differentiation of Data by
 487 Simplified Least Square Procedure. Anal. Chem, 44:1906–1909.

488 Ten Hallers-Tjabbes CC, Evaraarts JM, Mensink BP, Boon JP (1996) The decline of the North Sea
 489 whelk (*Buccinum undatum* L.) between 1970–1990: a natural or a human-induced event?
 490 Mar Ecol 17 (1–3):333–343

491 Valentinsson D, Sjodin F, Jonsson PR, Nilsson P, Wheatley C (1999) Appraisal of the potential for a
 492 future fishery on whelks (*Buccinum undatum*) in Swedish waters: CPUE and biological
 493 aspects. Fish Res 42:215–227

494 Warton DI, Duursma RA, Falster DS, Taskinen S (2015) R- Package ‘smatr’ (standardised) Major Axis
 495 Estimation and Testing Routines

496 Weetman D, Hauser L, Bayes MK, Ellis JR, Shaw PW (2006) Genetic population structure across a
 497 range of geographic scales in the commercially exploited marine gastropod *Buccinum*
 498 *undatum*. Mar Ecol Prog Ser 317:157–169

499 Wheeler AP (1992) Mechanisms of molluscan shell formation. In: Bonucci E (ed) Calcification in
 500 biological systems. CRC Press, Boca Raton, pp 179–216.

501 Wilbur, K. M., Saleuddin, A. S. (1983) Shell formation. In. Wilbur, K. M. (ed.) The Mollusca -
 502 physiology. Vol. 4. Academic Press, New York, pp 235-237

503

504

505

506

507

508

509

510

511

512

513

514

515

516

517

518

519

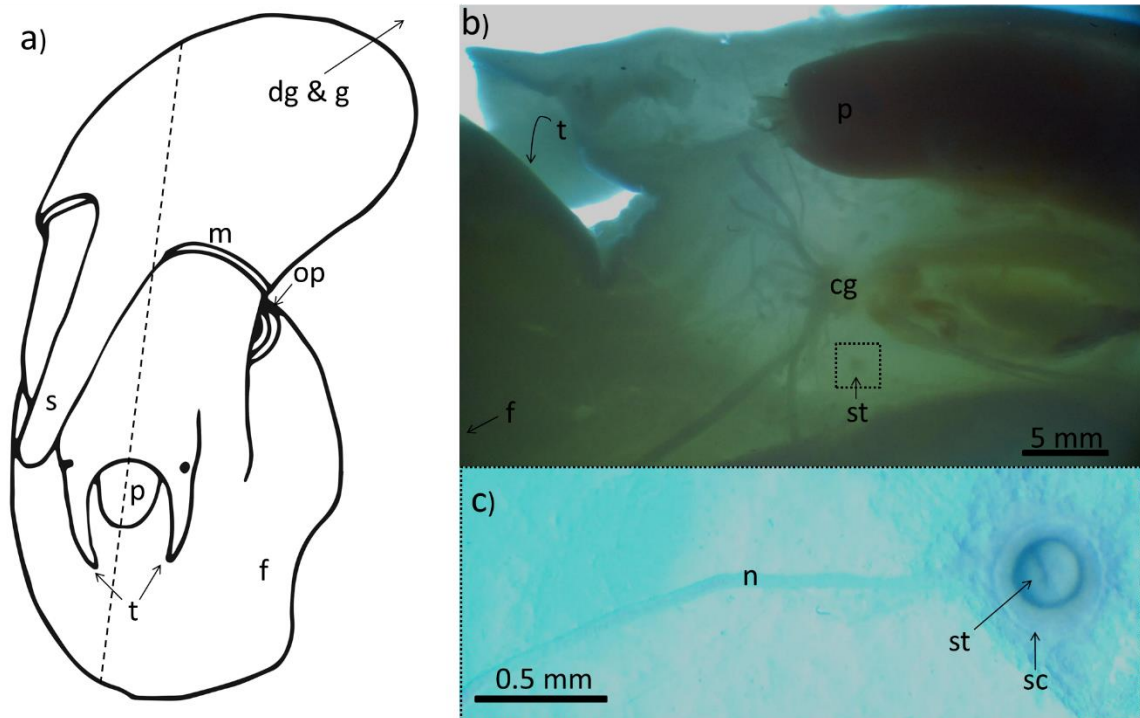
520

521

522

523

524



526

527 Figure 1. a) ventral view of a female *Buccinum undatum* removed from its shell showing; s - Siphon,
 528 m - Mantle, p - Proboscis, op - Operculum, f - Foot and t - Tentacles. dg - Digestive Gland and g -
 529 Gonad are out of frame. The dashed line represents the bisection of the whelk. b) half a bisected *B.*
 530 *undatum* illuminated using transmitted light, viewed in a dissection microscope, showing the cg -
 531 Cerebral Ganglion and st - Statolith. Dotted line represents area of interest shown in c). c) a statolith
 532 following removal; n - Nerve, st - Statolith and sc - Statocyst.

533

534

535

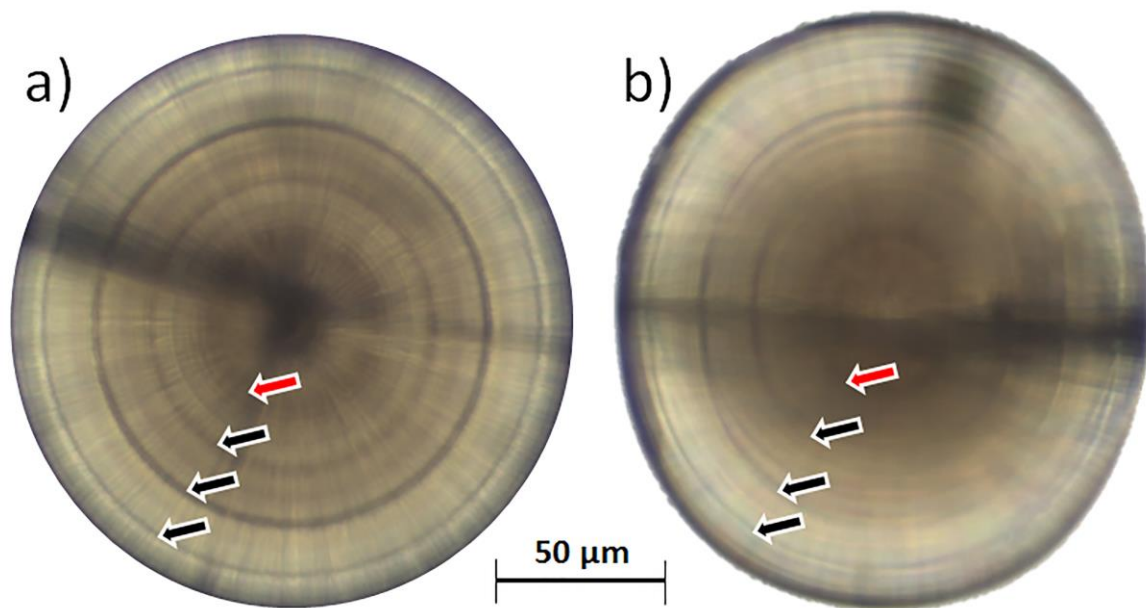
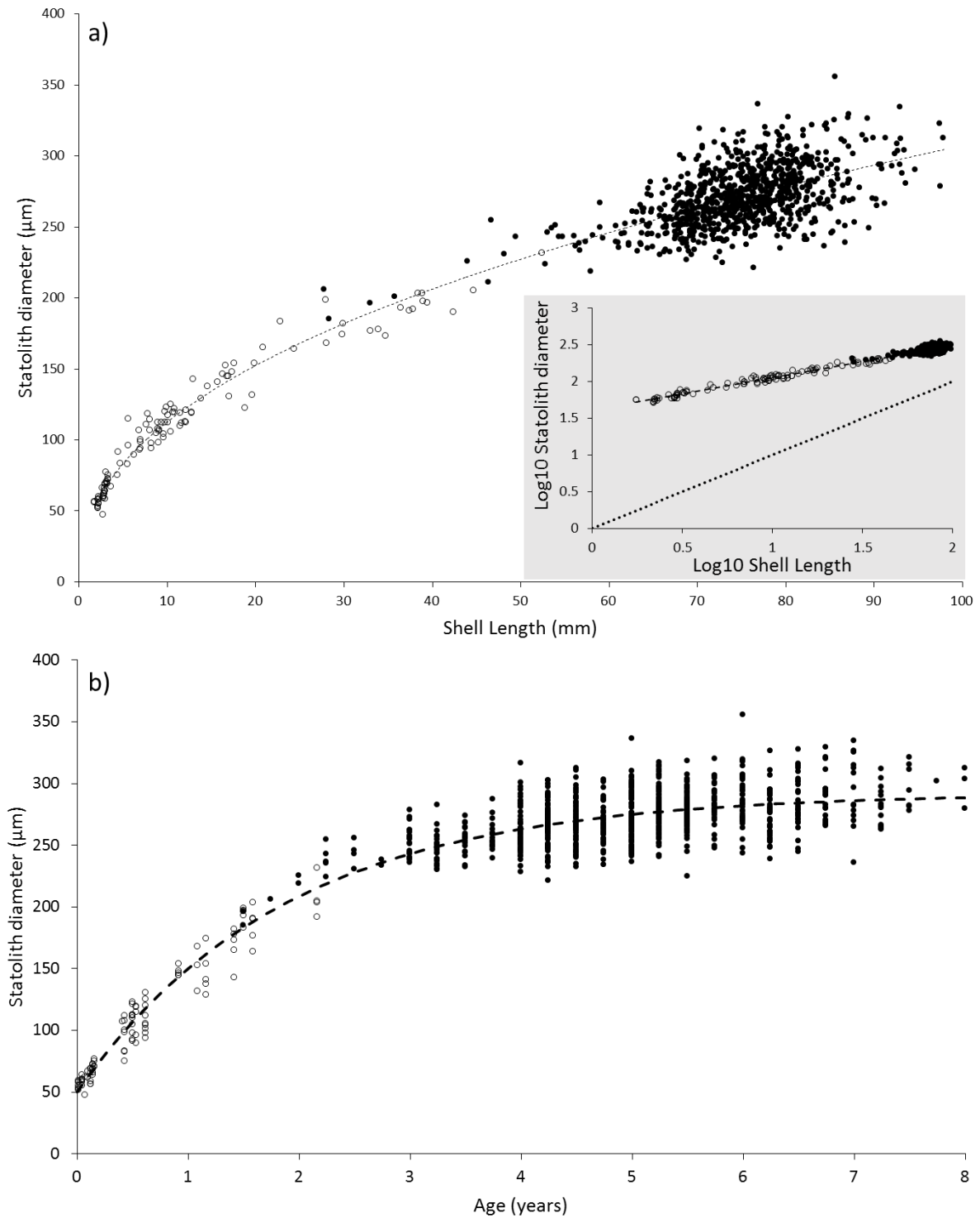


Figure 2. Photomicrographs of two statoliths removed from an individual *Buccinum undatum* from the Menai Strait. a) shows a dorso-ventral view whilst b) shows a lateral view of the statolith. The annual growth rings are marked with arrows and hatching rings with red arrows in each statolith orientation.



542

543 Figure 3. a) the relationship between Shell length and Statolith Diamater (StD), showing field
 544 collected whelks (filled circles), and laboratory reared juveniles (empty circles), fitted with a power
 545 function line (dotted line, $y = 41.38 * x^{0.4354}$), $R^2 = 0.96$. 3a grey inset, scatterplot showing the
 546 relationship between log10 statolith diameter (StD) and log10 shell length (SL) of field collected
 547 *Buccinum undatum* from the Menai Strait (filled circles), and laboratory reared juveniles (empty
 548 circles). The slope of the linear relationship (dashed line) is 0.43 ($R^2 = 0.96$). The dotted line
 549 represents an isometric relationship. c) scatterplot showing the relationship between StD and age,
 550 constructed from statolith rings for field collected (filled circles) and laboratory reared animals of
 551 known age (empty circles), fitted with a von Bertalanffy growth curve, $R^2 = 0.90$. $n = 931$ for all plots.

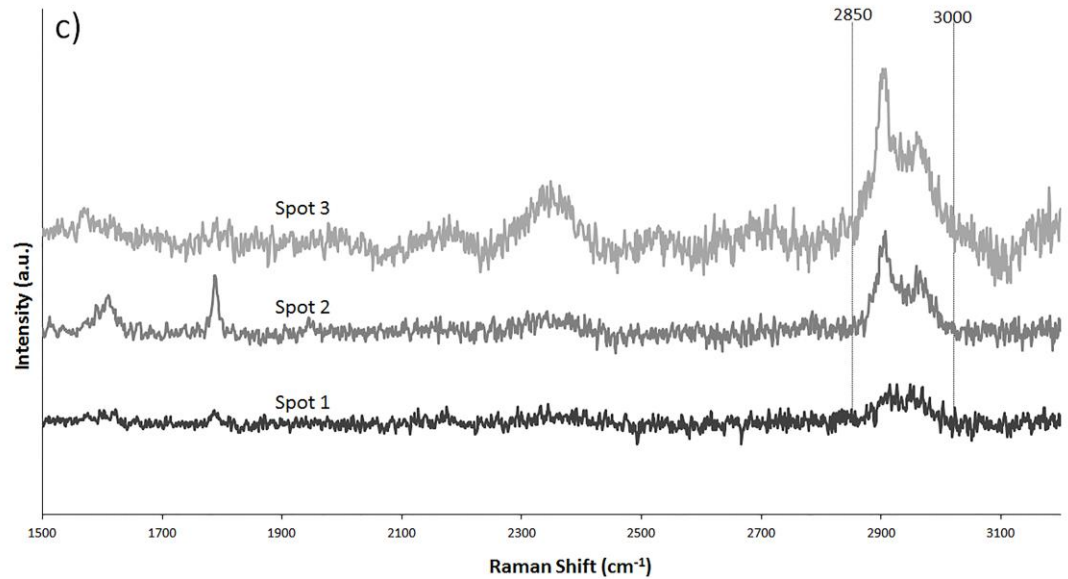
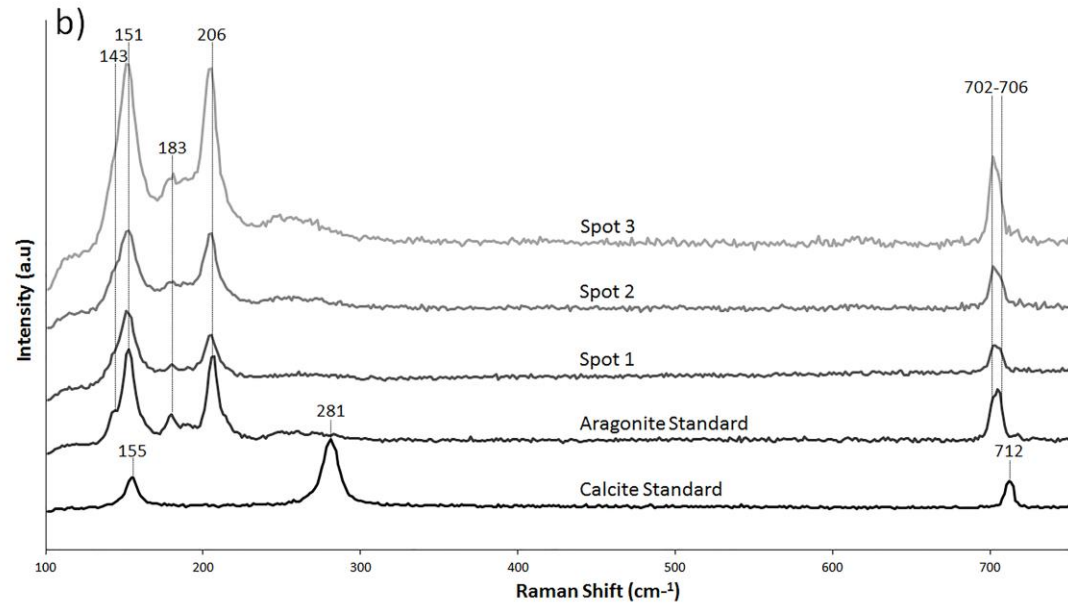
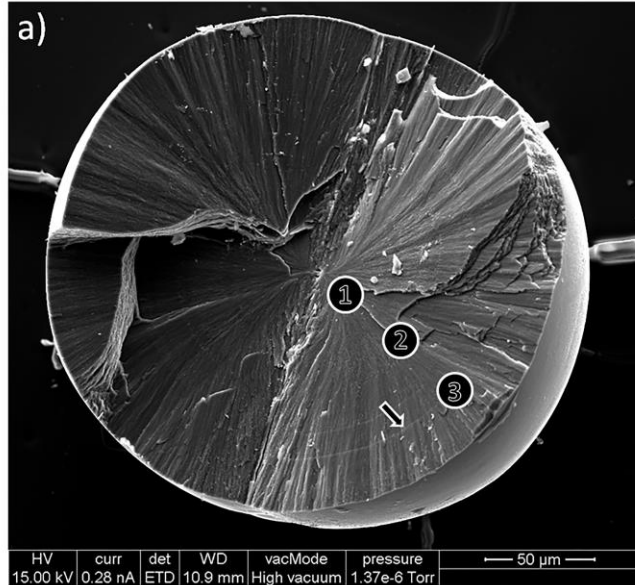
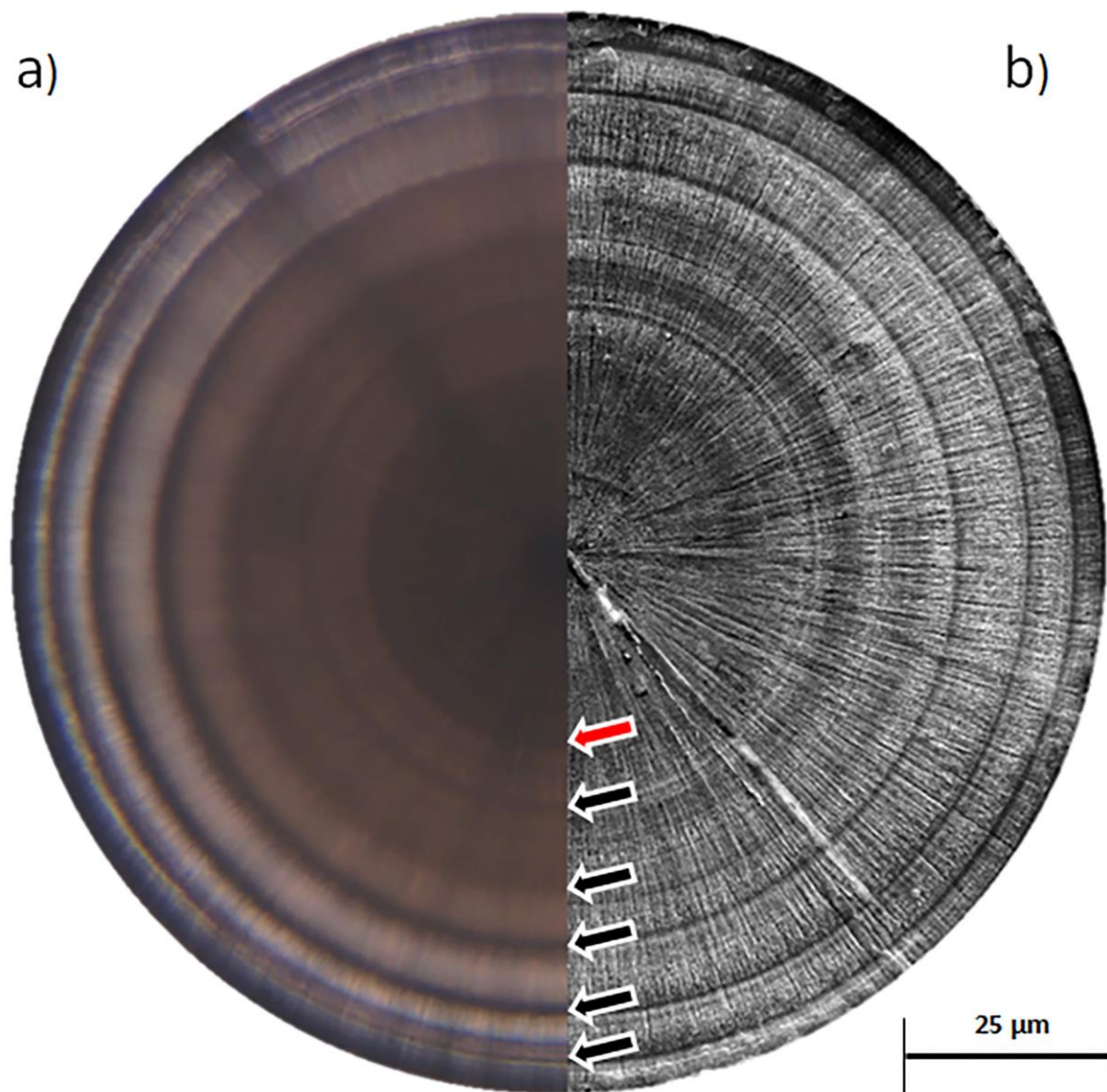
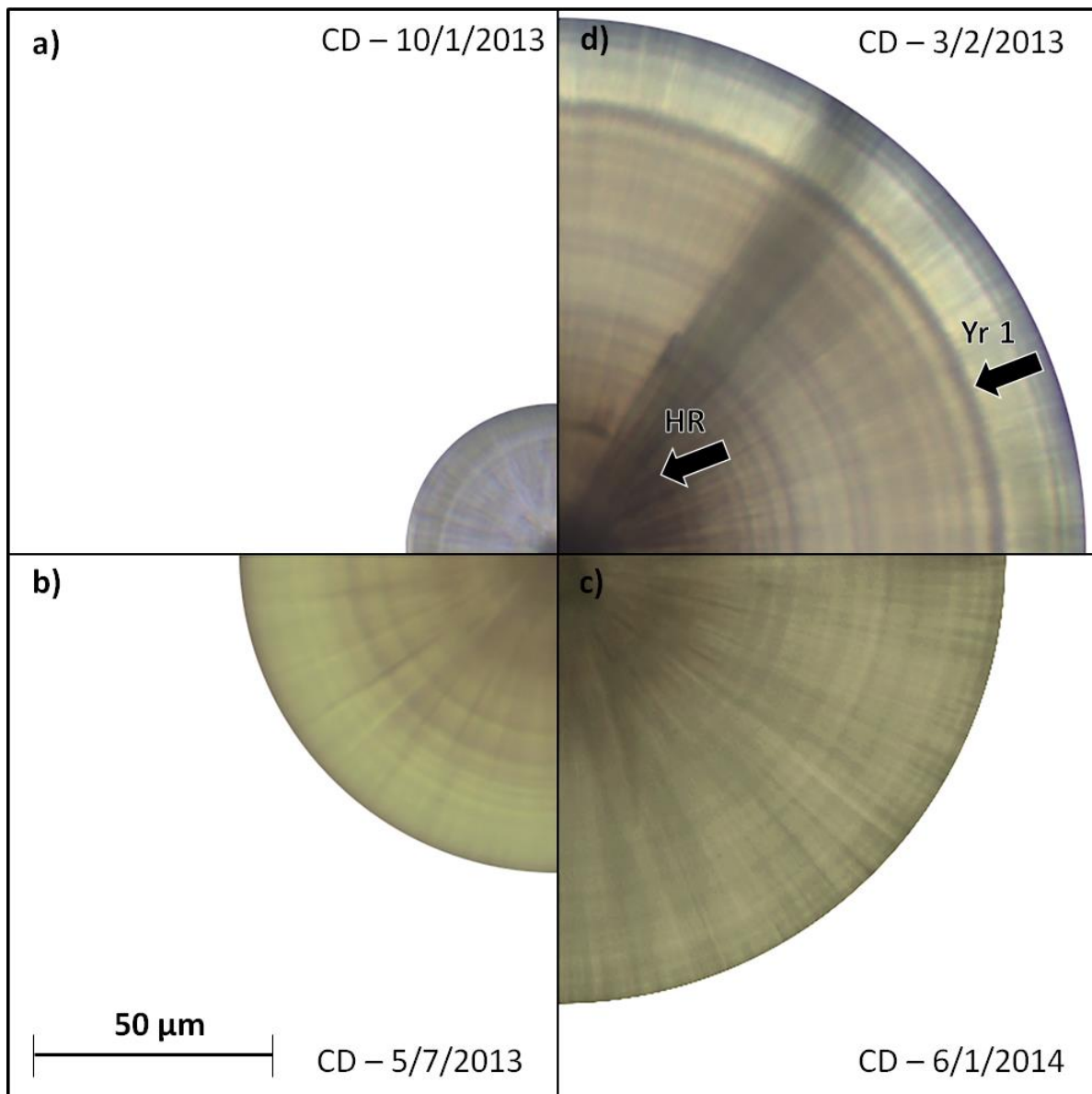


Figure 4a. Scanning electron microscope image of a cracked statolith with the central plane exposed. The sample spots used for micro-Raman analysis are shown with circles (1, 2 & 3). Arrow highlights a clear growth ring coincidentally sampled with spot 3. Figure 4b. Raman spectra from the 3 sample spots together with the aragonite and calcite standards. Raman spectra acquired from 100-750 cm^{-1} are displayed. Figure 4c. Raman spectra for the 3 sample spots extracted between 1500 and 3200 cm^{-1} (y axis presented as arbitrary units).



573

574 Figure 5. Composite image of two statoliths from the same *Buccinum undatum* specimen. a) a
 575 photomicrograph of an extracted and mounted left hand statolith imaged using optical microscopy.
 576 b), a Scanning Electron Microscope image of the matching right hand statolith that has been resin-
 577 mounted, ground to the central plane, polished and etched. Annual growth rings highlighted with
 578 black arrows, hatching ring highlighted with red arrow.



579

580 Figure 6. Composite image showing seasonal juvenile statolith development at a) 2 weeks after
 581 hatch, b) 6 months after hatch, c) 1 year after hatch and d) 2 years after hatch. In all cases the
 582 hatching ring is visible (HR) as are multiple faint disturbance lines. The 1 year ring is also visible in the
 583 2 year old (Yr 1). CD – Collection Date.

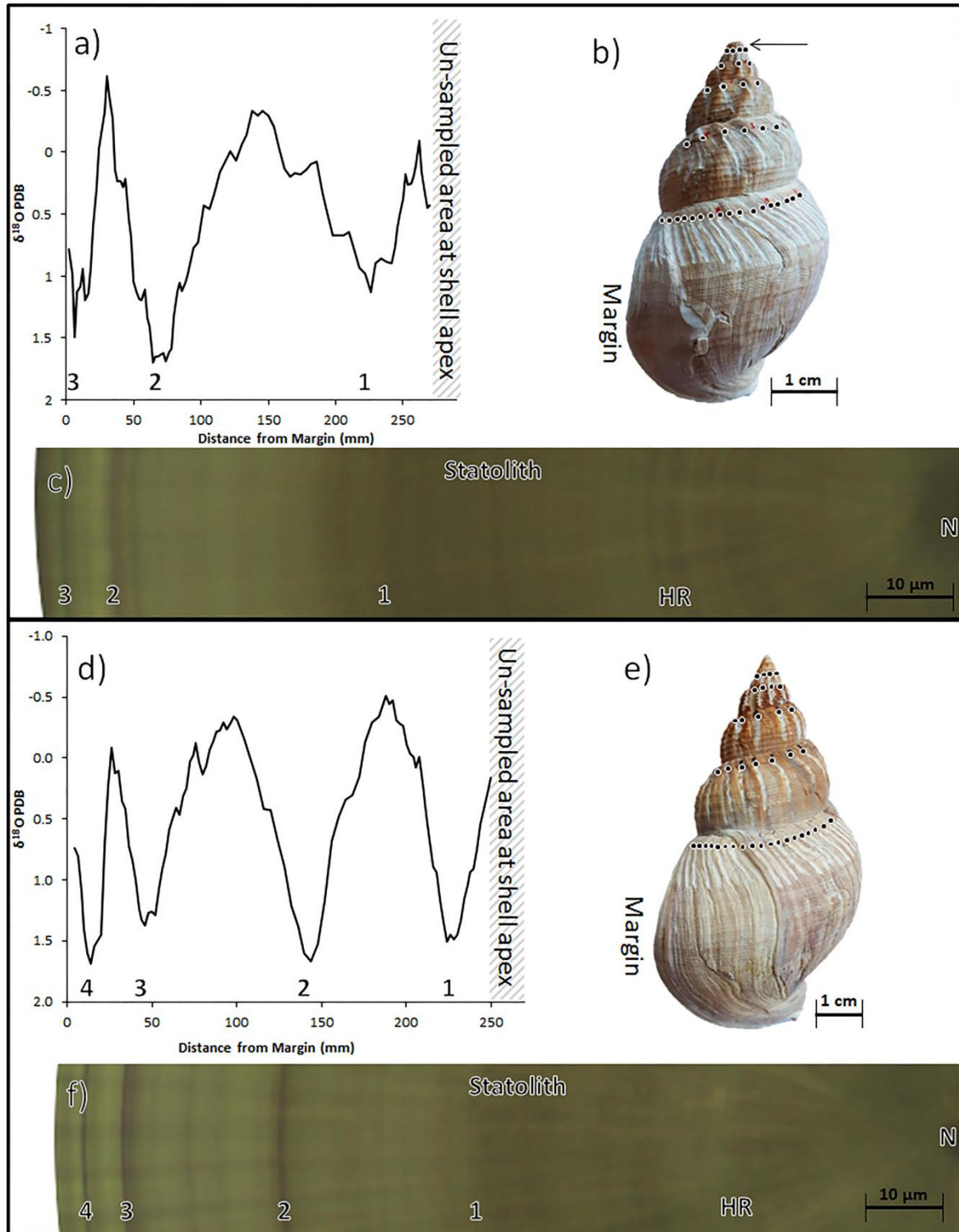


Figure 7. Comparison of the shell $\delta^{18}\text{O}$ profiles with the associated statolith for two *Buccinum undatum*. Figure 7a. $\delta^{18}\text{O}$ profile from the shell of a female *B. undatum*, the y axis has been inverted to show the position along the shell of the positive peaks in the $\delta^{18}\text{O}$ cycles (coldest seawater temperatures, highlighted with numbers). The data have been smoothed using 5 point Savitsky-Golay filter. Figure 7b. The shell drill sampled for the data in 7a, visible drill tracks have been highlighted with red dots and the black arrow denotes where sampling at the apex was ceased. This un-sampled area corresponds to the hatched area in 7a. The very tip of this specimen has been lost

592 due to damage. Figure 7c. Photomicrograph of the matching statolith from the animal in 7a & b,
593 showing the nucleus (N), Hatching ring (HR) and annual bands (numbers). Figure 7d, e & f show the
594 same figures as Figure 7a, b & c respectively for an older male specimen.